Resilin, the gene for the molecular spring: its roles in the flight and jumping of *Drosophila*

Miyuna Hagiwara[1], Yoshiki Eto[2], Yoko Keira[2], Hiroyuki O. Ishikawa[2],

Kensuke Aizawa[1], Takaomi Sakai[1], Toshiro Aigaki[1], Tsunaki Asano[1,*]

[1] Department of Biological Sciences, Tokyo Metropolitan University

[2] Department of Biology, Chiba University

*Corresponding Author: asano-tsunaki@tmu.ac.jp, Minami Osawa 1-1, Hachioji city, Tokyo, Japan

Email: asano-tsunaki@tmu.ac.jp

Tell: +81-426-771-111

Fax: +81-426-772-559

Abstract

Resilin is a member of the chitin-binding protein family that was originally found as a major component of an elastic matrix present in insects. The knockdown of the gene for this protein in *Drosophila melanogaster* causes the characteristic downturned wing posture, and the knockdown flies cannot move their wings. The jump distance of the knockdown flies is around 50% shorter than that of the controls. Null mutant flies show the same phenotypes, which can be rescued by introducing a 4.7 kb genomic fragment harboring the whole coding region of *Resilin*. *In vitro* experiments have shown that the elasticity of the matrix made of Resilin is due to the dityrosine-mediated polymerization of Resilin molecules. Dual oxidase (Duox) is the most likely candidate for the *in vivo* polymerization of Resilin molecules. *Duox* knockdown induces phenotypes similar to those observed in wing posture and jump performance of the *Resilin* knockdown and knockout flies, which can be rescued by the overexpression of *Duox* gene from a beetle. These findings suggest that Duox is an essential factor for the proper function of Resilin as the major component of the resilin matrix.

Introduction

Insects are often regarded as the most successful animals on Earth with their extreme diversity, enormous biomass, and great impact on the global ecosystem. There have been intensive debates as to why insects have been so successful, and their ability to fly must have had great impacts on their evolutionary process and the expansion of their habitat to a wide range of terrestrial environments. It is considered that the ability to fly is advantageous in the competition for survival and the creation of new niches not easily accessible to other animals, which is supported by the fact that 99% of the described insect species are winged.

During powered flight, insects flap their wings by moving their flight muscles in the thorax. Repetitive and rapid contractions of flight muscles are transformed into high-frequency wing motion, generating a force to lift the insect's body[1,2]. The hinges connecting the wings and the body have thick tendons, which may be involved in energy transformation from the flight muscles to the wings[3,4]. Accumulation of mechanical loads derived from the high-frequency vibration during flight could eventually destroy structures around the wing hinges. However, the thick tendon of the

wing hinges is composed of a rubber-like matrix, which may presumably absorb/relieve such stresses, and prevent the hinges from breaking down[3,4,5]. In addition to their powered flight, insects may also use the properties of such rubber-like matrices for jumping. Similarly to flight, jumping is a high-velocity locomotion through the air, which may be another advantage of insects that is not found in other invertebrates, with only a few exceptions of some arthropods, such as sand hoppers or jumping spiders[6,7,8]. It has been reported that the rubber-like matrices are found in the joints of the hind legs of the grasshopper or in the pleural arch at the top of the hind legs of the flea, both of which are positioned in places that can be easily imagined to be used for jumping. It has been proposed that the rubber-like matrices act as a spring during jumping.

The first description of the rubber-like matrices in insects was the discovery of tendons in the wing hinges of dragonflies and locusts[4]. At that time, the rubber-like matrices were named “resilin” after the Latin word, “resilire,” which means resilience, and were defined as materials that can be stained with methylene blue or toluidine blue. After that, rubber-like matrices (hereafter, referred to as the “resilin matrix”) were

65 found in the salivary pump and feeding pump of bags, or the tymbal of cicadas for

66 sound production[9,10]. The connection between jumping mechanisms and the

67 localization of the resilin matrix at leg joints has also been discussed in detail also in

68 insects such as grasshoppers that have the thick resilin matrix at the joints of their

69 hindlegs[11,12]. Relatively recent reports on the functions of the resilin matrix include

70 examples from bed bugs and midges. Male common bedbugs (*Cimex lectularius* and

71 *Cimex hemipterus*) puncture the intersegmental membrane of the female abdomen with

72 a needle to inject their sperm. After the male detaches from the female, the pore is

73 likely closed probably owing to the elasticity of the resilin matrix[13,14]. Larvae of the

74 phantom midge (*Chaoborus americanus*) can regulate their buoyancy by altering the

75 volume of their air sacs. This is achieved through a pH-dependent transition in the

76 shape of the resilin matrix that composes the air sacs. During this process, membrane

77 ATPase controls the proton content of the resilin matrix[15].

78 The physical properties of the resilin matrix are not affected considerably by

79 deep freezing, high temperature, or treatments with alcohols or fixatives. In contrast,

80 the resilin matrix is rapidly dissolved by proteolytic digestion, indicating that proteins

81 are its major constituents[4]. Subsequently, a study showed that proteins in the resilin

82 matrix are crosslinked together through the formation of di- or tri-tyrosine, in which

83 tyrosine residues are covalently crosslinked to each other[16]. It was also shown that di-

84 and tri-tyrosine emit the characteristic blue fluorescence under UV irradiation, and this

85 property has been used as a useful tool to observe the localization of the resilin matrix

86 noninvasively (hereafter, di- and tri-tyrosine are collectively referred to as dityrosine).

87 In 2001, Ardell and Andersen reported a candidate gene encoding a protein composing

88 the resilin matrix. Partial amino acid sequences of peptides isolated from the protease

89 digest of the resilin matrix taken from of the desert locust *Schistocerca greraria* were

90 determined by Edman degradation. The obtained sequences were used for BLAST

91 search in the genomic database of the fruit fly *Drosophila melanogaster* to find

92 candidate genes encoding *Drosophila* proteins homologous to the locust proteins[17].

93 Two proteins (CG15920 and CG9036) were found to have the sequences that matched

94 well with those obtained from the resilin matrix of the locust. On the basis of similarity

95 in amino acid compositions (high amounts of proline, glycine, and tyrosine), Ardell &

96 Andersen concluded that CG15920 was the most likely candidate, and tentatively

97 named the *CG15920 "Resilin*" as the gene for a major protein composing the resilin

98 matrix. Since that study, *CG15920* has been called *Resilin* (hereafter, *Rsl*). Until

99 recently, however, there had been no reports on the gene function analysis to directly

100 demonstrate that the gene encoding resilin is actually involved in insect flight or

101 jumping. Furthermore, it was also not known how resilin molecules are polymerized *in*

102 *vivo*, although *in vitro* experiments using a recombinant Rsl protein of *D. melanogaster*

103 have shown that Rsl polymerization is necessary for the high elasticity of synthetic

104 resilin matrix[5,18-20].

105 Here, using the newly obtained *Rsl* mutant of *D. melanogaster*, we characterized

106 the phenotypes and showed that *Rsl* has roles in preventing the breakdown of the wing

107 hinge structure over time and in efficient jumping. We also tried to show which genes

108 were involved in the polymerization of the Rsl molecule. Dual oxidase (Duox) is a

109 membrane protein with the extracellular peroxidase domain and the transmembrane

110 NADPH-oxidase domain. By tissue-specific *Duox* knockdown and its rescue

111 experiment, we showed that duox was indeed the factor for Rsl polymerization. We

112 also showed that the duox-mediated polymerization of Rsl was indispensable for the

113 proper function of the Rsl/resilin matrix both in flight and jumping, which may be the

114 critical factors for the evolution and success of insects as terrestrial organisms.

115 **Results**

116 **Gene structure of *Rsl***

117 *Rsl* locates at the cytogenetic position of 53D (right arm of the 2nd chromosome), and

118 it has two splicing isoforms, *Rsl-RA* and *Rsl-RB* (with and without exon 2,

119 respectively) (Fig. 1A)[21,22]. Rsl is the secreted protein with a signal sequence (Fig.

120 1B)[17]. The polypeptide encoded by *Rsl-RA* is divided into three parts: 1) repeats of

121 N-terminally located "elastic modulus", 2) chitin-binding motif, and 3) repeats of

122 C-terminally located "elastic modulus". The polypeptide encoded by *Rsl-RB* is devoid

123 of the large portion of the chitin-binding motif (Fig. 1B)[17,23].

124 The elastic moduli[23] (hereinafter referred to as elastic repeats) that are indicated

125 by light-blue or light-green boxes in Fig. 1B are characterized by the consensus

126 sequences containing proline, glycine, and tyrosine. The consensus sequences are also

127 found in other insect proteins that are annotated as resilin[22,23]. The tyrosine residue is

128 considered important for the formation of intermolecular crosslinks[17]. As first

129 described by Ardell and Andersen[17], the consensus sequences of the elastic repeats in

130 the N- and C-terminal regions are different from each other (Fig. 1B). In *D.*

131 *melanogaster*, the N-terminal repeats (-**P**--<u>Y</u>G-**P**G---) have two prolines with an

132 intervening tyrosine, whereas the C-terminal repeats (G<u>Y</u>S-GR**P**GG) have only one

133 tyrosine and one proline. In the multiple sequence alignment[22,23], the N-terminal

134 repeats are conserved among species, but there are at least two subtypes in the

135 consensus sequences of the C-terminal repeats. In many insects, the consensus is

136 G<u>Y</u>**P**SGG**P**GG with two prolines (type-A repeat). In contrast, many fly species and a

137 portion of hemipteran insects have the different consensus sequences characterized by

138 the presence of only one proline (Fig. 1B). In a comprehensive database search of

139 arthropod genomes, we found that in amino acid sequences of resilins from the

140 palaeopteran insects (Odonata and Ephemeroptera: the orders of the most primitive

141 winged insects) or those from the primitive non-insect hexapods such as collembolans,

142 no consensus sequences of the C-terminal repeats are found (Supplementary Fig. S1).

143 Considering the branching pattern of the phylogenetic tree illustrating the evolutionary

144 process of insects (see Supplementary Fig. S1), it can be hypothesized that the

145 C-terminal repeats are a trait that was obtained in accordance with the emergence of a

146 new type of winged insects (Neoptera). In the three-dimensional model of *Drosophila*

147 Rsl (Q9V7U0 in the uniplot database), which was predicted using AlphaFold Server

148 (https://alphafoldserver.com) powered by AlphaFold3[24] (Fig. 1C), both the N- and

149 C-terminal regions have a spring-like "coiled" shape (panels b and c, respectively),

150 with each elastic repeat corresponding to one cycle of the spring (panels d and e). The

151 presence of the beta turn at the short PGG sequence motif in the C-terminal repeats

152 (arrowheads in panel c) is consistent with the previous prediction[17]. The spring-like

153 shape of the Rsl model is intriguing, considering the function of the resilin as the

154 component of spring-rubber-like biomaterials.

155

156 **Expression of *Rsl***

157 In previous studies of the two Drosophilidae species[21,25], it was shown that *Rsl* was

158 mainly expressed in late pupal stages. Also in our RT-PCR analysis similar results were

159 obtained (Fig. 2A). The apparent signals of the isoforms *Rsl-RA* and *Rsl-RB* were

160 detected from the pupal to early adult stages. From 2 to 4 days after puparium

161 formation (APF), the signals for *Rsl* expressions are strong, and the emergence of the

162 signal for the expression of *Rsl-RB* precedes that of *Rsl-RA*. In western blotting with

163 the specific antibody, two signals corresponding to the molecular masses of 57k and

164 52k can be seen (Fig. 2B). The upper and lower signals correspond to mature Rsl-PA

165 and Rsl-PB without a signal sequence, respectively (Supplementary Fig. S2). The

166 emergence of the Rsl-PB signal precedes that of Rsl-PA, which is consistent with the

167 temporal patterns obtained by RT-PCR analysis (Fig. 2A). Rsl signals almost disappear

168 after eclosion, which is consistent with the observation that resilin molecules are

169 polymerized to become insoluble materials[16]. Rsl cannot penetrate into the SDS-PAGE

170 gel and are not detectable by western blot analyses.

171 To see the spatial patterns of *Rsl* expression, we prepared the *Rsl* promoter-Gal4

172 driver that covers of the genomic region around 2.3 kbp upstream of the first ATG (Fig.

173 1A). The expression was visualized using the *UAS-Rsl-RA*::*mCherry* reporter. The

174 photos in Fig. 2C show pupae on day 3 APF. The mCherry signal was visible at the

175 hinges of the wings, spiracles, compound eyes, legs, and labrum (Fig. 2C, panels a, b,

176 and c). In the observation of the adult on day 3 after eclosion, the mCherry signal can

177 be seen on the ventral side of the leg joints between the trochanter and the femur, and

178 the roots of the mechanosensory hairs of the leg and wing (Figs. 2D and 2E). These

179 expression patterns were obtained using flies carrying the *Rsl*-promoter Gal4 sequence

180 integrated into the 3rd chromosome. The mCherry signal pattern obtained with the

181 *Rsl*-promoter Gal4 sequence on the second chromosome was nearly identical to the

182 data obtained with *Rsl*-promoter Gal4 on the third chromosome, except that no signal

183 was observed in the compound eyes (Supplementary Fig. S3). In western blot analysis

184 of the compound eye (Fig. 2F) the signals of Rsl can be seen in the wild-type fly, and

185 this signal disappeared in the sample from Rsl^{KO} that we generated (Supplementary Fig.

186 S4). The results of the western blot analysis indicate that the signal in the wild-type fly

187 corresponds to Rsl, and that the compound eye surely expresses *Rsl*.

188 To observe the details of the internal structure at the wing hinge, we removed the

189 outer cuticle. The mCherry signal was clearly visible just beneath the wing hinge (Fig.

190 2G, panel i), and the structure exhibited blue fluorescence under UV irradiation (Fig.

191 2H). The intensity of this blue fluorescence signal decreased markedly and increased

192 under acidic and alkaline conditions, respectively (see Supplementary Fig. S5),

193 consistent with the characteristics of dityrosine previously reported[16]. This structure,

194 which is positive for both the mCherry signal and blue fluorescence, is the tergopleural

195 tendon. Previous studies have shown that this tendon is the structure connecting the

196 direct muscle and the root of the wing at the wing hinge[26-28].

197 Since Rsl-PA has the chitin-binding domain, we consider that this domain may

198 function in chitin binding. To visualize the distribution of the chitin fiber inside the

199 tergopleural tendon, we expressed ChtVis-tdTomato with *Rsl*-promoter-Gal4. Along

200 the horizontal midline, a strong signal can be seen, indicating the presence of chitin

201 along the midline (Fig. 2I). This is similar to the spatial pattern of Rsl-RA::mCherry

202 (Fig. 2H). Next, we compared the distributions of Rsl-RA::mCherry and

203 Rsl-RB::mCherry (with and without the sequence of the chitin-binding domain,

204 respectively) that were separately expressed (Fig. 2J). The spatial pattern of

205 Rsl-RA::mCherry, which is denser along the horizontal central line (panel p), contrasts

206 with the more uniform distribution of Rsl-RB::mCherry (panel q). Figure 2J, panel r

207 shows the calculated values of the biased distribution of mCherry signals (see

208 Materials and Methods). In this analysis, the value for the biased distribution was

209 higher in flies expressing Rsl-RA::mCherry than in those expressing Rsl-RB::mCherry,

210 indicating a more uniform distribution of Rsl-RB::mCherry, which may be caused by

211 the absence of a chitin-binding domain.

212

213 **Phenotypes by the defect of *Rsl* expression**

214 To examine the effects of the suppression of *Rsl* expression, we knocked down *Rsl*[29]

215 with the *Rsl*-promoter Gal4 driver, and the expression was suppressed to around the

216 baseline levels (Supplementary Fig. S6). In the *Rsl* knockdown flies, no visible

217 phenotypes were observed in the very early stages of the adult, but after one day, all

218 the knockdown individuals were unable to move their wings and started to display the

219 characteristic downturned wing posture (Fig. 3A). The same wing posture has been

220 observed in multiple studies including the analysis of *pink1*, which functions in muscle

221 development[30,31]. The phenotypes observed in our *Rsl* knockdown are the same as

222 those previously reported for the *Rsl* knockdown flies[21]. To further characterize the

223 function of *Rsl*, we used the null mutant (Rsl^{KO}) that was prepared in this study

224 (Supplementary Fig. S4). The homozygous Rsl^{KO} flies showed the characteristic

225 downturned wing posture, and they could not move their wings, which are the same

226 phenotypes as those observed in *Rsl* knockdown flies (Fig. 3C, see Supplementary mov.

227 S2). To rescue these phenotypes, we generated flies with the transgene of the 4.7 kbp

228 genomic fragment harboring the *Rsl* coding region on the 3rd chromosome

229 (*Rsl*-Genomic rescue: *Rsl-GR*) (Fig. 1A). The Rsl^{KO} flies with *Rsl-GR* did not show the

230 downturned wing posture (Figs. 3C and 3D), and they could move their wings and fly

231 (see Supplementary mov. S3), indicating that *Rsl-GR* rescued the phenotypes of Rsl^{KO}.

232 Then, we also tried to rescue the phenotypes of Rsl^{KO} using the Gal4/UAS system (Fig.

233 3D). Although flies expressing each isoform only gradually showed the wing posture

234 phenotype, the phenotype was almost rescued. Combining the two isoforms did not

235 show markedly different results with those obtained from either *Rsl-RA* or *Rsl-RB*

236 alone.

237 It was shown in *D. melanogaster* that the tergopleural tendon was stained with

238 the anti-Rsl antibody[27], which is consistent with the presence of the signal for the

239 Rsl::mCherry reporter at the tergopleural tendon (Figs. 2G and 2H). In Fig. 3E, we

240 illustrated the structure around the tergopleural tendon on the basis of the photo of the

241 wing hinge from the wild-type flies, and also according to the previous descriptions

242 [27,28]. In this observation, *dumpy-YFP* (*dpy-YFP*) was used to visualize the boundary

243 between the tendon and the muscle. The green signal of Dpy-YFP surrounds the resilin

244 matrix as shown by the blue fluorescence emitted upon UV irradiation (Fig. 3E, panel

245 a). The proximal side of the tergopleural tendon is attached to the root of the wing

246 hinge (indicated by the white arrowhead). The direct flight muscles (tergopleural

247 muscles 1 and 2: TP-1 and TP-2, respectively) are attached to the tergopleural tendon.

248 In the photo of the newly eclosed Rsl^{KO} fly (Fig. 3E, panel b), no blue fluorescence

249 signal of dityrosine was seen. The loss of dityrosine signals can be explained by the

250 absence of Rsl, which is supposed to provide the tyrosine residues as the source of

251 dityrosine. As shown in panel b of Fig. 3E, the tergopleural tendon of the newly

252 emerged Rsl^{KO} fly remained linked to the root of the wing (closed arrowheads), which

253 may correlate with the absence of wing posture or movement abnormalities (Fig. 2D).

254 In contrast, in Rsl^{KO} flies exhibiting the downturned wing posture (panel c), the

255 tergopleural tendon was ruptured into two pieces (white arrows), confirming the loss of

256 connection between the muscle and the root of the wing. In Rsl^{KO} flies with *Rsl-GR*

257 (panel d), the blue fluorescence that is surrounded by the Dpy-YFP signal is clearly

258 visible. The structures of TP-1 and TP-2 are the same as those observed in wild-type

259 flies, and no damage was observed. This is consistent with the *Rsl*^{KO} flies with *Rsl-GR*

260 showing no phenotypes of wing posture and movement abnormalities (Figs. 3C and

261 3D; Supplementary mov. S3).

262 In the fields of anatomy and biomechanics, many reports define "resilin" as an

263 extracellular structure that exhibits blue fluorescence, which is characteristic of

264 dityrosine[32]. The blue fluorescence signal has been found in various body parts,

265 including the intersegmental membrane, compound eyes, and wings[33,34]. In this study,

266 we examined the *Rsl*^{KO} fly to confirm whether the blue fluorescence disappears in the

267 absence of *Rsl*. We focused on the wings, since the presence of the blue fluorescence

268 signal in wings has been reported in multiple insect species[33,34]. As shown in

269 Supplementary Fig. S7B, the arrows indicate distinct blue fluorescence signals at the

270 proximal part of the wing, roughly corresponding to the area with landmarks adopted

271 in a previous study[35]. These signals became weak drastically under acidic conditions,

272 suggesting that they corresponded to dityrosine. However, the wing of the *Rsl*^{KO} fly

273 still showed a clear blue fluorescent signal (see Supplementary Fig. S7D), supporting

274 an idea that dityrosine-rich structures exist without Rsl in *D. melanogaster*.

275

276 **Polymerization of Rsl by *Duox***

277 It has been shown that Duox is involved in dityrosine formation in ecdysozoans such

278 as nematodes and insects[36-38]. The ROSs produced in the peroxidase domain may

279 oxidize a tyrosine residue to form a tyrosine phenoxyl radical, followed by the reaction

280 with the neighboring tyrosine residue to produce dityrosine or trityrosine[36,37]. Duox

281 may be the most plausible candidate factors responsible for Rsl polymerization,

282 because Rsl molecules are polymerized through dityrosine formation[16]. To demonstrate

283 this, we examined the effect of *Duox* knockdown on Rsl polymerization or other

284 phenotypic characteristics. In this study, we performed tissue-specific *Duox*

285 knockdown with *Rsl-Gal4*, because whole body knockdown or knockout of *Duox* leads

286 to lethality[36,39]. Immediately after eclosion, *Duox* knockdown flies were able to fold

287 and move their wings normally, but within a day all of them exhibited the downturned

288 wing posture, similarly to *Rsl* knockdown and knockout (Figs. 4A and 4B). The *Duox*

289 knockdown flies could not move their wings, similarly to *Rsl* knockdown and

290 knockout flies. We used two UAS-lines, NIG stock #3131R-3 (*NIG3131R-3*) and

291 *UAS-Duox-RNAi*$_{976\text{-}1145}$[39], for *Duox* knockdown, and in both cases the same wing

292 phenotypes were obtained (hereafter, we mainly performed phenotypic characterization

293 using NIG3131R-3).

294 To examine the cause of the downturned wing posture in *Duox* knockdown flies,

295 we performed western blot analysis to determine whether Rsl molecules were

296 polymerized. As shown in Fig. 4C, the signal of Rsl remained detectable after eclosion

297 (Fig. 4C). This is in contrast to the patterns of the control (Fig. 4C) and wild-type flies

298 (Fig. 2B), in which the Rsl signals disappeared after eclosion. In the *Duox* knockdown

299 flies, the signal for Rsl can be seen at the same electrophoretic mobility of Rsl

300 monomers (Fig. 4C), indicating that a portion of Rsl molecules remained

301 unpolymerized.

302 We also observed the structure around the tergopleural tendon of the *Duox*

303 knockdown flies (Fig. 4D). In the control flies (panels a and b), the structures were

304 almost the same as those of the wild type (Fig. 3E), as can be judged from the presence

305 of the blue fluorescence signal at the tergopleural tendon. In the *Duox* knockdown flies,

306 the signal for dityrosine in the tergopleural tendon (indicated by the dotted line in panel

307 c) was very weak (panels a and b). In the *Duox* knockdown flies, the TP-1 and TP-2

308 were completely detached from the tergopleural tendon with the signal of Dpy (panel

309 e), as illustrated in panel f.

310 To rescue the phenotypes caused by *Duox* knockdown, we prepared a UAS-line

311 for expressing of *T. castaneum Duox* (*TcDuox*) as a transgene with a base sequence that

312 is not similar to that of *D. melanogaster Duox*. As shown in Fig. 4E, *Duox* knockdown

313 flies with additional *TcDuox* expression did not exhibit the downturned wing posture,

314 even one week after eclosion (Figs. 4E and 4F). The flies could move their wings

315 normally and fly (our observation). In western blot analysis, the Rsl signal disappeared

316 within two days after eclosion (Fig. 4G, right panel), in contrast to the control flies in

317 which the Rsl signal remained detectable even after two days (left panel). The

318 anatomical structure around the tergopleural tendon was almost the same as that of the

319 wild type (Fig. 4H, right panel), which can be judged from the presence of the blue

320 fluorescence signal in the tergopleural tendon, and also the connection between the

321 tergopleural tendon and TP muscles (TP-1 and TP-2). These findings indicate that the

322 expression of *TcDuox* rescued the phenotypes of the *Duox* knockdown flies, and that

323 *Duox* is the actual factor responsible for Rsl polymerization and the proper functioning

324 of Rsl/resilin matrix in the maintenance of the structure around the wing hinges. We

325 then examined biochemically the Duox-mediated Rsl polymerization through

326 dityrosine formation. Here, commercially available peroxidase was used as the catalyst,

327 instead of the peroxidase domain of Duox, because we were unable to successfully

328 synthesize the functional peroxidase domain of Duox. In the western blot analysis of

329 the truncated version of the recombinant Rsl (reRsl), which was synthesized in an *E.*

330 *coli* system, reRsl migrated at an electrophoretic mobility corresponding to the

331 predicted molecular mass of 35 k (Fig. 4I, left panel lane a). After treatment with either

332 peroxidase or hydrogen peroxide (lanes b and c), reRsl can be seen at its original

333 mobility. In contrast, in the presence of both peroxidase and hydrogen peroxide, the

334 reRsl signal was shifted to an electrophoretic mobility corresponding to a much higher

335 molecular mass (lane d). As indicated by closed arrowheads, the strong smear signal

336 was seen from the entry site of the concentration gel. The shift of the Rsl signal to an

337 electrophoretic mobility corresponding to high-molecular masses indicates that the Rsl

338 molecules formed a high-molecular mass complex. In the western blot analysis with

339 the antibody against dityrosine (right panel), signals are visible only in the sample

340 treated with both peroxidase and hydrogen peroxide (lane h). The signal is strongest at

341 the entry site of the concentration gel (closed arrowhead), indicating the presence of

342 reRsl that is highly polymerized by the formation of a large number of dityrosines.

343

344 **Phenotypes of jump performance**

345 It has been proposed that the resilin matrix may enable high performance in jumping in

346 several insects such as the flea and locust[21,40-42]. In this study, as a method to quantify

347 the jump performance in *D. melanogaster*, we measured the jump distance using

348 de-winged flies (Fig. 5A). In the control flies, their jump distance was around 2 cm,

349 but in the *Rsl* knockdown flies, their jump distance was shorter by around half of that

350 of the control (Fig. 5B). Also, in Rsl^{KO} flies, the jump distance was almost half of that

351 of the wild-type flies (Fig. 5C). The jump distance of the Rsl^{KO} flies with *Rsl-GR* was

352 almost the same as that of the wild-type flies (Fig. 5C), indicating that the phenotype

353 of shorter jump distance was rescued by *Rsl-GR*. In the rescue experiment using the

354 Gal4/UAS system, we were unable to obtain data clearly showing the successful rescue

355 with either *UAS-Rsl-RA* or *UAS-Rsl-RB*. Therefore, presently, we do not have

356 information on the functional differences in jumping between Rsl-PA and Rsl-PB (not

357 shown).

358 Here, in addition to *Rsl*, we examined the contribution of *Duox* to fly jumping.

359 *Duox* was knocked down with either of *NIG3131R-3* or *UAS-Duox-RNAi*$_{976\text{-}1145}$, and in

360 both cases, the jump distances of the knockdown flies were around half of that of the

361 controls (Fig. 5D). To rescue this phenotype, *TcDuox* was additionally expressed in the

362 *Duox* knockdown flies (*Rsl>NIG3131R-3*). With the expression of *TcDuox*, the jump

363 distance was increased to around twofold that of the *Duox* knockdown flies (Fig. 5E),

364 indicating that *TcDuox* expression compensated for the reduction in the level of the

365 endogenous *Duox* expression.

366

367 **Discussion**

368 Duox is the oxidase that is widely conserved in metazoans, and is also the thyroid

369 oxidase in mammals[43,44]. There have been many studies on the diverse roles of Duox,

370 including defense responses against intestinal wound, immune responses against

371 pathogens the regulation of stem cell development/differentiation, and extracellular

372 matrix formation[36-39,45-48]. In particular, in ecdysozoans such as insects and nematodes,

373 it is considered that the Duox-mediated crosslinking through dityrosine formation is

374 very important for the strengthening and stabilization of the extracellular matrix[36-38,49].

375 In this study, we showed that Rsl was polymerized by Duox, in which inter-Rsl

376 molecule dityrosine formation may occur (Figs. 4C, 4G, and 4I). In insects, this is the

377 first study to identify the target protein of the Duox-mediated polymerization. The

378 polymerization of Rsl may be used as a model of the formation of the dityrosine matrix,

379 which is distributed widely in metazoan taxa including annelids and molluscs[50,51].

380 Until this study, two reports on the function of the resilin-encoding gene in

381 Drosophilae species had been published, both by Moussian's group. Here, we were

382 able to specify the internal structures related to the emergence of this phenotype (Fig.

383 3F). As shown in Fig. 3F, the tergopleural tendon was ruptured in Rsl^{KO} flies. The

384 direct flight muscles (TP-1 and TP-2) that are linked to the tergopleural tendon are

385 required for the movement of the wings that are upturned, as has been demonstrated in

386 a neurogenetic experiment[52]. Probably, in the *Rsl* knockdown and Rsl^{KO} flies, the

387 tergopleural tendon may have been damaged owing to the accumulation of stress from

388 the wing movement, since the occurrence of this phenotype is time-dependent (Figs.

389 3B and 3D). After the rupture of the tergopleural tendon, energy transfer from the

390 muscle to the wings may no longer occur.

391 In the insect database of the full-length CDS or long-read RNA-seq results, we

392 found two splicing isoforms of resilins with or without the chitin-binding domain (our

393 observation), which indicates the possibility that presence of these two isoforms is

394 important. During the period of adult body development in *D. melanogaster*, the

395 emergence of the Rsl-PB isoform (without the chitin-binding domain) was faster than

396 that of the Rsl-PA isoform (Figs. 2A and 2B). The localization of Rsl-PA::mCherry

397 (with the chitin-binding domain) in the tergopleural tendon (Fig. 2H) is actually similar

398 to that observed in the distribution of chitin fibers that were visualized using the

399 ChtVis-tdTomato chitin reporter (Fig. 2I). This suggests that the chitin-binding domain

400 of Rsl-PA is functional *in vivo*, which is consistent with the finding of an *in vitro*

401 experiment using recombinant Rsl, showing the binding of the chitin-binding domain

402 to chitin[22]. The binding of the Rsl molecule to chitin fibers seems to have a certain

403 significance for the formation and proper functions of the tergopleural tendon.

404 However, when we compared the extent of phenotypic rescue by overexpressions of

405 *Rsl-RA* and *Rsl-RB* in Rsl^{KO} flies, the downturned wing phenotypes was rescued, in

406 almost the same proportion (Fig.3D). This suggests that the chitin-binding domain is

407 not necessarily required for Rsl functions at the wing hinge. In the measurements of

408 jumping, although the phenotype was rescued with *Rsl-GR* (Fig. 5C), the

409 Gal4/UAS-mediated expression of each isoform may have been insufficient to rescue

410 the shorter jump distance of Rsl^{KO} flies (not shown). Therefore, as described above, we

411 do not have information on the functional difference in jumping between the two

412 isoforms. In the wing hinge, it is possible that other cuticle proteins with both tyrosine

413 residues and the chitin-binding domain may compensate for the absence of the

414 chitin-binding ability of Rsl-PB by mediating the linkage between chitin fibers and

415 Rsl-PB.

416 The polymerization of elastic protein moieties often occurs to give the matrix

417 high elasticity, as seen in other elastic materials, such as elastin and abductin. *In vitro*

418 experiments designed to polymerize recombinant Rsls support this theory[5,19,53]. In

419 these studies, either peroxidase, photocatalysts, or chemical modifiers were used to
420 artificially polymerize Rsl, and the resulting materials treated with these reagents
421 exhibited high elasticity. The representative molecule forming the elastic matrix in
422 mammals is elastin, which is referred to as the "molecular spring" because of its roles
423 in restoring the structure and providing elasticity to tissues[53-55]. Elastin molecules can
424 extend eight times their original length and then recoil. The 3D model of Rsl predicted
425 using the AlphaFold Server resembles a coiled spring (Fig. 1C), suggesting a potential
426 role of Rsl as a molecular spring similarly to elastin. The tyrosine residues of Rsl may
427 form intermolecular crosslinks, which may be responsible for the formation of the
428 resilin matrix and its high resilience. According to the UniProt website
429 (https://www.uniprot.org/uniprotkb/Q9V7U0/entry), the chitin-binding domain of the
430 resilin model has a pLDDT score greater than 90, indicating high precision in the 3D
431 model prediction. However, the scores for the N- and C-terminal repeats are estimated
432 to be low (pLDDT score <70), which indicates that these regions could be intrinsically
433 disordered proteins. This is consistent with previous predictions that the Rsl molecule
434 has a random structure, lacking alpha helices or beta sheets[23,56]. However, low scores

435 in AlphaFold's predictions may simply reflect insufficient information about proteins
436 possessing similar sequences that could serve as references for known protein
437 structures during 3D modeling. At present, there is insufficient evidence to rule out the
438 possibility that Rsl possesses a structure similar to that of the predicted model. To
439 accurately understand the thermodynamic mechanism by which polymerized Rsl
440 molecules exhibit high elasticity, it would be beneficial to confirm whether Rsl
441 actually possesses a coil-like structure.

442 As shown in Fig. 4A, the knockdown of *Duox* induced the same downturned
443 wing posture as that of the *Rsl* mutant. This result can be explained by the failure of
444 Rsl polymerization, as shown in the western blot in Fig. 4C. Even in the adult stage,
445 Rsl polypeptides remained detectable at an electrophoretic mobility corresponding to
446 those of the Rsl monomers. The reduction or loss of the elasticity of the resilin matrix
447 at the tergopleural tendon may have occurred, finally leading to the rupture of the
448 tergopleural tendon. It is also possible that the link between the tergopleural tendon
449 and the muscle is lost probably because of the weak bonding between them, as can be
450 assumed from the detachment of the muscle from the tergopleural tendon (Fig. 4D).

451 *Duox* knockdown induced the reduction in the intensity of dityrosine signal in the

452 tergopleural tendon (Fig. 4I), strongly supporting the idea that Duox is the factor for

453 dityrosine-mediated Rsl polymerization.

454 The model that Duox is the factor for Rsl polymerization was based on the

455 studies of the nematode *Caenorhaboritis elegans* showing that the gene for Duox is

456 involved in the dityrosine-mediated polymerization of collagens in the cuticle

457 matrix[37,49]. It is possible that this process may be controlled by humoral factors,

458 because it is stage-dependent. It has been shown that the functions of Duox are

459 regulated by the EF-hand motif present at the intracellular part of this protein[39,45]. We

460 observed the increase in the cytosolic calcium level in the cells surrounding the

461 tergopleural tendon in the late pupal stages (our observation). The next step is to

462 clarify whether the increase in the cytoplasmic calcium level actually contributes to the

463 activation of Duox and the subsequent dityrosine formation, and to elucidate the

464 molecular mechanisms underlying the stage-dependent regulation of cytoplasmic

465 calcium for the activation of Duox to initiate the polymerization of resilin during the

466 process of adult development.

467 Regarding jumping, both *Rsl*^{KO} and *Duox* knockdown flies showed shortened

468 jump distances, indicating the loss of the polymerized Rsl may have been the cause of

469 this phenotype. We did not examine the changes in the intensity of the blue

470 fluorescence in *Rsl*^{KO} and *Duox* knockdown flies, because of the intense

471 autofluorescence around the structures of the leg joint. However, together with the data

472 of rescue experiments with *Rsl-GR* or overexpression of *TcDuox* (Fig. 5), it can be

473 thought that both the presence of Rsl and its polymerization are necessary for normal

474 jumping. In a recent study on the resilin gene of the locust, the authors showed the

475 lower jump performance of RNAi individuals (reduced jump velocity and irreversible

476 reduction in the jump distance during repetitive jumps)[57]. It was also shown that the

477 joints of the hind legs (between the femur and the tibia) were more easily broken in the

478 RNAi individuals. In *D. melanogaster*, the resilin matrix is present on the ventral side

479 of the leg joint (Fig. 2); from the finding, we proposed a simple model on how the

480 resilin matrix works in fly jumping (Supplementary Fig. S8). Before jumping, the

481 resilin matrix becomes tense to store mechanical energy, and when the fly jumps, the

482 stored energy may be liberated from the resilin matrix during transition to its relaxed

483 state.

484 As shown in the observation of the *Rsl*^{KO} flies, we found the wing structures still

485 showing blue fluorescence (Supplementary Fig. S7). The lack of Rsl is also supported

486 by the previous observation that there are no reporter signals at the proximal part of the

487 wing[21]. In many reports, the term 'resilin' has been used to refer to the cuticular or

488 other extracellular structures with blue fluorescence. However, the data from *Rsl*^{KO}

489 flies show the existence of the non resilin matrix with dityrosine, indicating that the

490 matrices positive for blue fluorescence do not necessarily contain Rsl molecules. It is

491 possible that such the non resilin matrix with blue fluorescence may have mechanical

492 properties quite different from those of the resilin matrix, because blue fluorescence

493 can be found in very hard parts such as the tip of the mandible of copepods or

494 ragworm[58,59]. Future studies will reveal the mechanical characteristics or composition

495 of the non resilin matrix with blue fluorescence and the biological significance of their

496 existence.

Methods

Fly stocks and maintenance

Fly stocks were reared at 25°C under a 12h light and dark cycle. They were fed the standard cornmeal‑agar‑glucose medium containing propionic acid and n-butyl p-hydroxybenzoate (7.21% cornmeal, 3.20% glucose, 8.01% yeast, and 0.64% agar supplemented with 9.9 mL/L butyl *p*-hydroxybenzoate and 3.0 mL/L propionic acid) . w^{1118} (our laboratory stock, Canton-S background) was used as the wild-type strain. *UAS-eGFP* (BL#1521), *UAS-GFP-RNAi* (BL#9331), *vas-int* (BL#40161), AttP2 (BL#36303), AttP5 (BL#34766), and *vas-Cas9* (BL#51323) were obtained from the Bloomington Drosophila Stock Center. *UAS-resilin-RNAi* (*KK106773*) in VIE260b (#101068) in was obtained from the Vienna Drosophila Resource Center. *UAS-Duox-RNAi* (#3131R-3) and $y^2cho^2v^1$*; Sco/CyO* (#TBX-0007) were obtained from Fly Stocks of the National Institute of Genetics. *UAS-Duox-RNAi*$_{976–1145}$[39] was kindly provided by Dr. Won-Jae Lee (Seoul National University, Korea). All mutants and lines that were used for knockdown were crossed into the w^{1118} control background for at least five generations.

RNA isolation and reverse-transcription PCR

Total RNA was extracted from individuals at each growth stage using RNAiso Plus (D9108A, Takara, Japan). cDNA was synthesized from 1 μg of total RNA using Prime Script RT Reagent Kit with gDNA Eraser (DRR047A, Takara). cDNAs were amplified using Prime star Max (R045A, Takara). To obtain patterns of stage-specific gene expressions, a three-step thermal cycling profile was used as follows: 95 °C for 1 min, followed by 25 cycles at 98 °C for 10 s, 55 °C for 5 s, and 72 °C for 5 s. The primers used in the RT-PCR are listed in Supplementary Table 1.

Generation of fly strains

Rsl^{KO} was obtained by the CRSPR/Cas9-mediated deletion of the whole coding region with two gRNAs[60]. The gRNAs were expressed from a transgene with a ubiquitous *pol III* promoter derived from *Drosophila snRNA:U6:96Ab*[61]. For construction of DNA to generate flies expressing gRNAs, two primer sets for *Rsl-gRNA1* and *-gRNA2* (listed in Supplementary Table 2) were annealed, and the resulting DNA fragments were

separately subcloned into *pBFv-U6.2* and *pBFv-U6.2B*, respectively, that were predigested with *Bbs*I. *pBFv-U6.2* with the sequence of *Rsl-gRNA1* was digested with *EcoR*I and *Not*I, and one of the resulting DNA fragments (with the sequence of *Rsl-gRNA1*) was ligated into one of the *EcoR*I and *Not*I fragment of *pBFv-U6.2B* (with the sequence of *Rsl-gRNA2*). The resulting vector with both the sequences for expressing *Rsl-gRNA1* and *-gRNA2* was introduced into AttP2 flies using a phiC31 integration system[60,61]. The flies with the transgene were crossed with *vas-Cas9* flies and the offspring were crossed with $y^2cho^2v^1$*; Sco/CyO* virgins to establish lines with deletions. The genotypes of the established lines were checked by genomic PCR analysis using the primers listed in Supplementary Table 2.

For the construction of the plasmid vector for generating transgenic flies (*Rsl-Gal4, Rsl* genomic rescue (*Rsl*-GR)*, UAS-Rsl-RA*, and *UAS-Rsl-RB*), genomic DNA and cDNA obtained from w^{1118} were used as templates of PCR. For the subcloning of the PCR fragments, an In-Fusion HD cloning kit (Z9648N, Takara) was used. To construct the vector of *Rsl-Gal4*, the 2.3 kbp PCR fragment for the *Rsl* promoter region amplified using the primer set (Supplementary Table 2) was subcloned into *pBPGw*

(Addgene; https://www.addgene.org/) that was predigested with *Kpn*I and *Bgl*II. To generate flies with the transgene for the genomic rescue of Rsl^{KO}, we prepared a 4.7 kb genomic fragment containing the *Rsl* CDS (from 1.0 kb upstream to 0.5 kb downstream of the transcription start and stop sites of *Rsl*), which was amplified by PCR using the primer set (Supplementary Table 2). The DNA fragment was subcloned into *pBFv-U6.2* predigested with *EcoR*I and *Not*I. For the construction of the plasmid vector to generate *UAS-Rsl-RA* and *UAS-Rsl-RB*, PCR fragments corresponding to the whole coding regions of *Rsl-RA* and *Rsl -RB,* respectively, were amplified using the primer set (Supplementary Table 2) with the cDNA. They were subcloned into *pUAST-attB* (laboratory stock) predigested with *Not*I and *Xba*I. For the construction of the vector for *UAS-TcDuox*, the DNA fragment corresponding to the whole coding region of the duox gene of the red flour beetle *Tribolium castaneum* was amplified by PCR using the *T. castaneum* cDNA and the primer set (Supplementary Table 2) (*T. castaneum* was a kind gift from Dr. Toru Togawa, Nihon University, Japan). For the construction of *UAS-Rsl-RA::mCherry* and *UAS-Rsl-RB::mCherry*, the whole coding region of each isoform was amplified by PCR using the primer set (Supplementary Table 2) with

cDNA from iso-1 (BL2057) as the template. A fragment including the sequence of mCherry with an N-terminal flexible 4 × GlyGlySer linker was PCR-amplified from *UASp-Elyssim-mCherry*[31] using the primer set (Supplementary Table 2). The two DNA fragments were subcloned into *Eco*RI fragment of *pUAST-attB* by the SLiCE method (Motohashi, 2015). Each vector was introduced into flies with AttP5 (*UAS-Rsl-RA, UAS-Rsl -RB,* and *UAS-Tcduox*) or AttP2 (*Rsl-Gal4*, *Rsl-GR, UAS-Rsl-RA::mCherry*, and *UAS-Rsl-RB::mCherry*) using a phiC31-based integration system[62,63].

Generation of antibody

A part of Rsl (Lys478-Gly590) was chosen as the antigen to raise the antibody against Rsl. In this study, pET-32 (Novagen, USA) was used to express the Rsl antigen as a fusion protein with the N-terminally located thioredoxin. The DNA fragment corresponding to the antigen was amplified with the primer set (Supplementary Table 1) using the cDNA of w^{1118}. The PCR product was digested with *Xho*I and *Bgl*II, and ligated into pET-32 predigested with the same enzyme set. The vector constructed was used to transform the *E. coli* BL21 strain. After the IPTG induction of the recombinant

protein expression (1 mM, 4 h of culture at 37°C), the *E. coli* cells were harvested by centrifugation, and ruptured by sonication in 50 mM Tris-HCl (pH 7.5) containing 150 mM sodium chloride. From the extract, the recombinant protein was purified by Ni-NTA affinity chromatography using Ni-NTA Agarose (30210, Qiagen, Germany). The N-terminally located thioredoxin was removed by thrombin treatment to break the peptide bond between the thioredoxin and the Rsl antigen, and the Rsl antigen was used for the immunization of a rabbit. The serum obtained from the rabbit was used as the anti-Rsl antibody.

Western blot analysis of fly samples

Five individuals at different stages (white pupae, pupae, and adults) were homogenized in 400 μL of 2×SDS-PAGE sample buffer (12.5 mM Tris at pH 6.8, 20% glycerol, 4% SDS, 2% 2-mercaptoethanol, and 0.001% bromophenol blue) and boiled for 10 min at 100°C. The proteins in a 5 μL aliquot were separated by SDS-PAGE using 12.5% polyacrylamide gel and transferred to PVDF membranes (IPFL00010, Merck KGaA, Germany). After blocking using 5% skim milk with TBST (0.1% Tween20), the

membranes were incubated with the rabbit anti-Rsl antibody (1: 3000 dilution) and mouse anti- α -Tubulin antibody [DM1A] (ab7291, Abcam, UK) (1: 5000 dilution) in Can Get signal solution 1 (NKB-201, Toyobo, Japan) at 4°C overnight. For the secondary antibody, IRDye-conjugated anti-rabbit and anti-mouse IgGs (925-68071 and 925-32210, respectively, LI-COR, USA) were used with Can Get signal solution 2 (NKB-301, TOYOBO, Japan) (1: 20000 dilution, for 2 h at 25°C). For luminescence imaging, an Odyssey DLx imaging system (LI-COR, USA) was used.

Measurement of jump distance

One day before the experiments, the flies were de-winged under mild CO_2 anesthesia. Jump distance was measured using the equipment, which was set in a room kept as 25°C. At the bottom of the glass beaker, 2% agarose was placed. After hardened, the agarose solution, a mesh for scaling was put on the agarose gel, and the surface was covered with additional 2% agarose. Five flies per group were housed in the equipment and their jumping were tracked for 5 minutes at 480 fps with Tough TG-5 (4545350-051112, OLYMPUS, Japan) and the jump distances were measured on the

basis of intervals of the mesh. The longest jump distance in each group was used as the representative value. The experiments were performed at least eight times for each genotype and sex.

Crosslinking of Rsl

Horseradish peroxidase was used for the crosslinking reaction of recombinant Rsl[20,64]. 100 μg of the recombinant Rsl (CSB-EP892693DLU, WUHAN HUAMEI BIOTECH, USA) was dissolved with 100 μl of 50 mM potassium phosphate buffer (pH7.0). Horseradish peroxidase (P-8375, Sigma, USA) was dissolved with 0.1 M potassium phosphate buffer (pH 6.0) to a final concentration of 20 μg/μL. 1 μL of the recombinant Rsl solution was mixed with 5 μL of 50 mM potassium phosphate buffer (pH 7.0). Then, 1 μL of horseradish peroxidase solution and 3 μL of 0.3% hydrogen peroxide (18084-00, KANTO CHEMICAL, Japan) were added, and the mixture was incubated at 30°C for 1 h. After incubation, the reaction mixture was mixed with 10 μL 2×SDS-sample buffer and boiled for 10 min at 100°C. Western blot analyses of Rsl and dityrosine were performed using the rabbit anti-Rsl antibody (this study) and the mouse monoclonal

anti-dityrosine antibody (MDT-020P, JaICA, Japan). The experimental procedures of western blot analysis were the same as those described in section 2.5.

Histology and microscopy

To observe the internal structure of the wing hinge, the adult thorax was divided into two parts (left and right) along the midline. Then the body parts around the wing hinge were obtained by trimming with microscissors. The tissues were fixed using 4% paraformaldehyde with PBS (pH 7.0). After blocking using 5% BSA (A7906, Merck KGaA) with PBST (0.05% Tween20), these samples were incubated in phaloidin-iFluor488 (CAY20549, Cayman Chemical, USA) with PBST (1:500) at 25°C overnight. An OLYMPUS BX60 (OLYMPUS, Japan) equipped with an WRAYCAM-VEX830 (WRAYMER, Japan) was used for whole-body or dityrosine, mCherry, and YFP signal detection. An OLYMPUS SZX7 (OLYMPUS, Japan) equipped with an OLYMPUS DP71 (OLYMPUS, Japan) was used for observing the phenotypes of wing posture.

2.9. Quantification of biased Rsl::mCherry distribution

The standard deviation (std) and the mean intensity of the mCherry signal in the resilin matrix were quantified using ImageJ. The std/mean was used as the index of the biased Rsl::mCherry distribution[65].

Statistical analyses

Statistical analyses were performed using R version 3.6.0 (https://www.r-project.org/). The Wilcoxon rank sum test was used to compare the jump distances. The student t-test was used to compare the intensities of mCherry signals in the resilin matrix in the wing hinges. The Steel‑Dwass test was used to compare the expression levels of *Rsl*, *Duox,* and *TcDuox*.

Acknowledgements

UAS-Duox-RNAi$_{976–1145}$ was a kind gift of Dr. Won-Jae Lee (Seoul National University, Korea). *T. castaneum* was a kind gift from Dr. Toru Togawa (Nihon University, Japan). We thank the National Institute of Genetics, the University of Indiana. Bloomington *Drosophila* Stock Center and the Vienna *Drosophila* Resource Center for providing fly lines. This work is supported by JSPS KAKENHI Grant Number JP23H02225 and 21J21904 and the Sasakawa Scientific Research Grant from The Japan Science Society.

Author contributions

M.H. and T.A. initiated, designed the experiments, and developed the project. M.H. performed all the experiments, analyzed the data, and prepared the figures. Y.E. and Y.K. generated *UASt-resilin-RA::mCherry* and *UASt-resilin-RB::mCherry*. K.A. firstly found the downturned wing phenotype of the *resilin* knockdown fly using *Actin-Gal4* in a preliminary experiment. M.H. and T.A. wrote and edited the manuscript. H.O.I., T.S., To.A. and T.A. reviewed the manuscript.

Competing interests

The authors declare no competing financial interests.

References

1. Ellington, C. P. The aerodynamics of hovering insect flight. VI. Lift and power requirements. *Philos. Trans. R. Soc. London. B, Biol. Sci.* **305**, 145–181 (1984).
2. Ellington, C. P. Power and efficiency of insect flight muscle. *J. Exp. Biol.* **VOL. 115**, (1985).
3. Andersen, S. O. & Weis-Fogh, T. Resilin. A Rubberlike Protein in Arthropod Cuticle. *Adv. In Insect Phys.* **2**, 1–65 (1964).
4. Weis-Fogh, T. A Rubber-Like Protein in Insect Cuticle. *J. Exp. Biol.* **37**, (1960).
5. Elvin, C. M. *et al.* Synthesis and properties of crosslinked recombinant pro-resilin. *Nature* **437**, 999–1002 (2005).
6. Parry, D. A. & Brown, R. H. J. The Hydraulic Mechanism of the Spider Leg. *J. Exp. Biol.* **36**, 423–433 (1959).
7. Wan, C., Hao, Z. & Feng, X. Structures, properties, and energy-storage mechanisms of the semi-lunar process cuticles in locusts. *Sci. Reports 2016 61* **6**, 1–13 (2016).
8. Wan, C. & Gorb, S. N. Body-catapult mechanism of the sandhopper jump and its biomimetic implications. *Acta Biomater.* **124**, 282–290 (2021).
9. Bennet-Clark, H. C. Negative Pressures Produced in the Pharyngeal Pump of the Blood-Sucking Bug, Rhodnius Prolixus. *J. Exp. Biol.* **40**, 223–229 (1963).
10. Young, D. & Bennet-Clark, H. C. The Role of the Tymbal in Cicada Sound Production. *J. Exp. Biol.* **198**, 1001–1020 (1995).
11. Lyons, R. E. *et al.* Molecular and functional characterisation of resilin across three insect orders. *Insect Biochem. Mol. Biol.* **41**, 881–890 (2011).
12. Burrows, M. Development and deposition of resilin in energy stores for locust jumping. *J. Exp. Biol.* **219**, 2449–2457 (2016).
13. Stutt, A. D. & Siva-Jothy, M. T. Traumatic insemination and sexual conflict in the bed bug Cimex lectularius. *Proc. Natl. Acad. Sci. U. S. A.* **98**, 5683–5687 (2001).
14. Michels, J., Gorb, S. N. & Reinhardt, K. Reduction of female copulatory damage by resilin represents evidence for tolerance in sexual conflict. *J. R. Soc. Interface* **12**, (2015).
15. McKenzie, E. K. G., Kwan, G. T., Tresguerres, M. & Matthews, P. G. D. A pH-powered mechanochemical engine regulates the buoyancy of Chaoborus midge larvae. *Curr. Biol.* **32**, 927-933.e5 (2022).
16. Andersen, S. O. The cross-links in resilin identified as dityrosine and trityrosine. *BBA -*

Gen. Subj. **93**, (1964).

17. Ardell, D. H. & Andersen, S. O. Tentative identification of a resilin gene in Drosophila melanogaster. *Insect Biochem. Mol. Biol.* **31**, 965–970 (2001).
18. Balu, R., Dutta, N. K., Dutta, A. K. & Choudhury, N. R. Resilin-mimetics as a smart biomaterial platform for biomedical applications. *Nat. Commun. 2021 121* **12**, 1–15 (2021).
19. Li, L. & Kiick, K. L. Resilin-based materials for biomedical applications. *ACS Macro Lett.* **2**, 635–640 (2013).
20. Qin, G. *et al.* Recombinant exon-encoded resilins for elastomeric biomaterials. *Biomaterials* **32**, 9231–9243 (2011).
21. Lerch, S. *et al.* Resilin matrix distribution, variability and function in Drosophila. *BMC Biol.* **18**, 1–15 (2020).
22. Ohkubo, S., Shintaku, T., Mine, S., Yamamoto, D. S. & Togawa, T. Mosquitoes Possess Specialized Cuticular Proteins That Are Evolutionarily Related to the Elastic Protein Resilin. *Insects* **14**, 941 (2023).
23. Andersen, S. O. Studies on resilin-like gene products in insects. *Insect Biochem. Mol. Biol.* **40**, 541–551 (2010).
24. Abramson, J. *et al.* Accurate structure prediction of biomolecular interactions with AlphaFold 3. *Nature* **630**, 493–500 (2024).
25. Lerch, S., Yang, Y., Flaven-Pouchon, J., Gehring, N. & Moussian, B. Resilin is needed for wing posture in Drosophila suzukii. *Arch. Insect Biochem. Physiol.* **111**, e21913 (2022).
26. Neff, D. Bursicon, Metamorphosis and Development of Resilin in the Fruit Fly. *Theses, Diss. Capstones* (2012).
27. Wong, D. C. C., Pearson, R. D., Elvin, C. M. & Merritt, D. J. Expression of the rubber-like protein, resilin, in developing and functional insect cuticle determined using a Drosophila anti-rec 1 resilin antibody. *Dev. Dyn.* **241**, 333–339 (2012).
28. Fabian, B., Schneeberg, K. & Beutel, R. G. Comparative thoracic anatomy of the wild type and wingless (wg1cn1) mutant of Drosophila melanogaster (Diptera). *Arthropod Struct. Dev.* **45**, 611–636 (2016).
29. Dietzl, G. *et al.* A genome-wide transgenic RNAi library for conditional gene inactivation in Drosophila. *Nat. 2007 4487150* **448**, 151–156 (2007).
30. Greene, J. C. *et al.* Mitochondrial pathology and apoptotic muscle degeneration in

Drosophila parkin mutants. *Proc. Natl. Acad. Sci. U. S. A.* **100**, 4078–4083 (2003).

31. Park, J. *et al.* Mitochondrial dysfunction in Drosophila PINK1 mutants is complemented by parkin. *Nature* **441**, 1157–1161 (2006).
32. Michels, J., Appel, E. & Gorb, S. N. Functional diversity of resilin in Arthropoda. *Beilstein Journal of Nanotechnology* (2016) doi:10.3762/bjnano.7.115.
33. Appel, E., Heepe, L., Lin, C. P. & Gorb, S. N. Ultrastructure of dragonfly wing veins: Composite structure of fibrous material supplemented by resilin. *J. Anat.* **227**, 561–582 (2015).
34. Michels, J. & Gorb, S. N. Detailed three-dimensional visualization of resilin in the exoskeleton of arthropods using confocal laser scanning microscopy. *J. Microsc.* **245**, 1–16 (2012).
35. Gidaszewski, N. A., Baylac, M. & Klingenberg, C. P. Evolution of sexual dimorphism of wing shape in the Drosophila melanogaster subgroup. *BMC Evol. Biol.* **9**, 1–11 (2009).
36. Anh, N. T. T., Nishitani, M., Harada, S., Yamaguchi, M. & Kamei, K. Essential role of duox in stabilization of Drosophila wing. *J. Biol. Chem.* (2011) doi:10.1074/jbc.M111.263178.
37. Edens, W. A. *et al.* Tyrosine cross-linking of extracellular matrix is catalyzed by Duox, a multidomain oxidase/peroxidase with homology to the phagocyte oxidase subunit gp91phox. *J. Cell Biol.* (2001) doi:10.1083/jcb.200103132.
38. Hurd, T. R., Liang, F. X. & Lehmann, R. Curly Encodes Dual Oxidase, Which Acts with Heme Peroxidase Curly Su to Shape the Adult Drosophila Wing. *PLOS Genet.* **11**, e1005625 (2015).
39. Ha, E. M., Oh, C. T., Bae, Y. S. & Lee, W. J. A direct role for dual oxidase in Drosophila gut immunity. *Science (80-.).* **310**, 847–850 (2005).
40. Burrows, M., Shaw, S. R. & Sutton, G. P. Resilin and chitinous cuticle form a composite structure for energy storage in jumping by froghopper insects. *BMC Biol.* **6**, 1–16 (2008).
41. Burrows, M. & Sutton, G. P. Locusts use a composite of resilin and hard cuticle as an energy store for jumping and kicking. *J. Exp. Biol.* **215**, 3501–3512 (2012).
42. Sutton, G. P. & Burrows, M. Biomechanics of jumping in the flea. *J. Exp. Biol.* **214**, 836–847 (2011).
43. De Deken, X. *et al.* Cloning of Two Human Thyroid cDNAs Encoding New Members of the NADPH Oxidase Family. *J. Biol. Chem.* **275**, 23227–23233 (2000).

44. Dupuy, C. *et al.* Purification of a novel flavoprotein involved in the thyroid NADPH oxidase. Cloning of the porcine and human cDNAs. *J. Biol. Chem.* (1999) doi:10.1074/jbc.274.52.37265.

45. Ha, E. M. *et al.* Coordination of multiple dual oxidase–regulatory pathways in responses to commensal and infectious microbes in drosophila gut. *Nat. Immunol. 2009 109* **10**, 949–957 (2009).

46. Lee, K. A. *et al.* Bacterial-derived uracil as a modulator of mucosal immunity and gut-microbe homeostasis in drosophila. *Cell* **153**, 797–811 (2013).

47. Moreira, S., Stramer, B., Evans, I., Wood, W. & Martin, P. Prioritization of Competing Damage and Developmental Signals by Migrating Macrophages in the Drosophila Embryo. *Curr. Biol.* **20**, 464–470 (2010).

48. Niethammer, P., Grabher, C., Look, A. T. & Mitchison, T. J. A tissue-scale gradient of hydrogen peroxide mediates rapid wound detection in zebrafish. *Nat. 2009 4597249* **459**, 996–999 (2009).

49. Thein, M. C. *et al.* Combined Extracellular Matrix Cross-linking Activity of the Peroxidase MLT-7 and the Dual Oxidase BLI-3 Is Critical for Post-embryonic Viability in Caenorhabditis elegans. *J. Biol. Chem.* **284**, 17549–17563 (2009).

50. Suderman, R. J., Dittmer, N. T., Kramer, K. J. & Kanost, M. R. Model reactions for insect cuticle sclerotization: Participation of amino groups in the cross-linking of Manduca sexta cuticle protein MsCP36. *Insect Biochem. Mol. Biol.* **40**, 252–258 (2010).

51. Kumar, S., Molina-Cruz, A., Gupta, L., Rodrigues, J. & Barillas-Mury, C. A peroxidase/dual oxidase system modulates midgut epithelial immunity in anopheles gambiae. *Science (80-.).* **327**, 1644–1648 (2010).

52. O'Sullivan, A. *et al.* Multifunctional Wing Motor Control of Song and Flight. *Curr. Biol.* **28**, 2705-2717.e4 (2018).

53. Carvajal, M. F. C. A. *et al.* Dynamics in natural and designed elastins and their relation to elastic fiber structure and recoil. *Biophys. J.* **120**, 4623–4634 (2021).

54. Jamhawi, N. M., Koder, R. L. & Wittebort, R. J. Elastin recoil is driven by the hydrophobic effect. *Proc. Natl. Acad. Sci. U. S. A.* **121**, e2304009121 (2024).

55. Trębacz, H. & Barzycka, A. Mechanical Properties and Functions of Elastin: An Overview. *Biomol. 2023, Vol. 13, Page 574* **13**, 574 (2023).

56. Qin, G., Hu, X., Cebe, P. & Kaplan, D. L. Mechanism of resilin elasticity. *Nat. Commun.*

3, (2012).

57. Rogers, S. M. *et al.* RNAi of the elastomeric protein resilin reduces jump velocity and resilience to damage in locusts. *Proc. Natl. Acad. Sci. U. S. A.* **122**, e2415625121 (2025).
58. Birkedal, H. *et al.* Halogenated veneers: Protein cross-linking and halogenation in the jaws of Nereis, a marine polychaete worm. *ChemBioChem* **7**, 1392–1399 (2006).
59. Michels, J., Vogt, J. & Gorb, S. N. Tools for crushing diatoms - Opal teeth in copepods feature a rubber-like bearing composed of resilin. *Sci. Rep.* **2**, 1–6 (2012).
60. Kondo, S. & Ueda, R. Highly Improved gene targeting by germline-specific Cas9 expression in Drosophila. *Genetics* **195**, 715–721 (2013).
61. Wakiyama, M., Matsumoto, T. & Yokoyama, S. Drosophila U6 promoter-driven short hairpin RNAs effectively induce RNA interference in Schneider 2 cells. *Biochem. Biophys. Res. Commun.* **331**, 1163–1170 (2005).
62. Bischof, J., Maeda, R. K., Hediger, M., Karch, F. & Basler, K. An optimized transgenesis system for Drosophila using germ-line-specific ϕC31 integrases. *Proc. Natl. Acad. Sci. U. S. A.* **104**, 3312–3317 (2007).
63. Groth, A. C., Fish, M., Nusse, R. & Calos, M. P. Construction of transgenic Drosophila by using the site-specific integrase from phage phiC31. *Genetics* **166**, 1775–1782 (2004).
64. Qin, G. *et al.* Expression, cross-linking, and characterization of recombinant chitin binding resilin. *Biomacromolecules* **10**, 3227–3234 (2009).
65. Zhang, X. *et al.* Mechanoresponsive regulation of myogenesis by the force-sensing transcriptional regulator Tono. *Curr. Biol.* **34**, 4143-4159.e6 (2024).

Figure legends

Figure 1. Exon–intron organization in the *Rsl* locus and protein structures of Rsl. (A) From the top, schematic of the *Rsl* locus in the wild-type and Rsl^{KO} flies; the regions chosen to generate the transgenes for the rescue experiments (*Rsl-GR*) and for the Gal4 driver (*Rsl-Gal4*) are shown. Black and white boxes are CDSs and UTRs, respectively.

Two gRNAs designed for the deletion of CDS to generate Rsl^{KO} flies are indicated by short bars. The exon compositions of the two isoforms are shown at the bottom. (B) Domain-motif organization of Rsl isoforms are shown. Each of the functional domain or consensus is shown below. Rsl-PB has a small portion of the chitin-binding R&R consensus sequence (red box) encoded by the 5' part of exon 3. (C) The 3D model of Rsl-PA predicted in AlphaFold Server is shown. Panel a is the whole Rsl-PA model. Blue and green parts are the N-terminal and C-terminal repeats, respectively. In panels b and c, the N-terminal and C-terminal repeats are enlarged with their proline and tyrosine residues illustrated by blue and purple colors, respectively. In panel c, beta turns are indicated by closed arrowheads. Panels d and e show the views in which two repeats are extracted from panels b and c, respectively, with schematics for two cycles of their polypeptide backbones.

Figure 2. Temporal patterns of *Rsl* expression and spatial patterns of the reporter. (A) RT-PCRs of *Rsl-RA* and *Rsl-RB* from embryo to day 5 adult are shown. (B) Western blots of the Rsl protein from white pupa to day 5 adult are shown. In both A and B, FL,

WL, WP, P1-4, and A0-5 are the abbreviations of feeding larva, wandering larva, white pupa, pupa days 1−4, and adult day 0−5, respectively. (C−H and J) Spatial distribution of the Rsl-RA::mCherry reporter expressed with *Rsl-Gal4*. (C) Panels a – c show the views from dorsal, lateral, and ventral directions, respectively. In each panel, photos on the left side awere taken under white light. (D and E) The midleg of the flies (D) and the edge of the wing (E) are shown. Photos of the mCherry signal and bright field were merged. Scale bar: 50 µm. (F) The western blots of Rsl in the compound eyes dissected from day-3 pupae of the wild-type and Rsl^{KO} flies are shown. The electrophoretic mobilities of Rsl-PA and Rsl-PB are indicated with arrowheads. (G) The Rsl-RA::mCherry localization at the wing hinge is shown. The outer cuticle was removed together the wing (arrowhead) to observe the internal structure (panel h). In panel i, the area enclosed in the square in panel h is enlarged. Scale bar: 500 µm. (H) Panel j is the magnified view of the wing hinge of the fly expressing *Rsl-RA::mCherry*. Panel k is the photo taken under UV radiation, and panel l is the merged photo of the panels j and k. Scale bar: 50 µm. (I) The distribution pattern of ChtVis-tdTomato that was expressed with *Rsl-Gal4* is shown. Scale bar: 50 µm. In both H and I, the

wavelengths of the filters used for excitation and the detection of dityrosine are 330−385 and >420 nm, respectively. (J) The biased distributions of Rsl::mCherry signals are compared. Panels p and q are the photos of the resilin matrix visualized with Rsl-RA::mCherry and Rsl-RB::mCherry, respectively. In panel r, the deviations of the biased distribution were calculated as described in Materials and Methods.

Figure 3. Phenotypes of *Rsl* knockdown and mutant flies. (A) The wing postures of the control fly (left: *Rsl>GFP-RNAi*) and *resilin* knockdown fly (right: *Rsl>Rsl-RNAi*) are compared. Scale bar: 0.5 mm. (B) The proportion of flies with normal wing posture on each day against the total number of flies is indicated (closed circles: *Rsl>GFP-RNAi*, grey circles: *Rsl>Rsl-RNAi*). (C) The wing postures of wild-type (w^{1118}), Rsl^{KO} (w^{1118}; Rsl^{KO}), and rescued (w^{1118}; $resilin^{KO}$; *resilinGR*) flies are compared. Scale bar: 0.5 mm. (D) The temporal changes in the proportion of flies with normal wing posture after eclosion are shown. The fly genotypes are w^{1118} (closed circles), $resilin^{KO}$ (gray circles), $resilin^{KO}$; *resilinGR* (open circles), $resilin^{KO}$; *resilin-Gal4* (closed triangles), $resilin^{KO}$, *UAS-resilin-RA* (gray triangles), $resilin^{KO}$, *UAS-resilin-RB* (open triangles),

resilin^{KO},UAS-resilin-RA; resilin-Gal4 (closed squares), *resilin^{KO},UAS-resilin-RB; resilin-Gal4* (gray squares), and *Rsl^{KO},UAS-Rsl-RA/Rsl^{KO},UAS-Rsl-RB*; *Rsl-Gal4* (open squares). (E) The inner structure of the wing hinge in *Dpy-YFP* was observed (panel a, left part), and its schematic is shown (right part). The red signals indicate muscles stained with phalloidin. The blue signal corresponds to blue fluorescence emitted upon UV irradiation. Green signals indicate Dpy-YFP. White arrow heads indicate the cuticle structure beneath the wing hinge attached to the proximal end of the tergopleural tendon. According to a previous study, two direct flight muscles, TP1 and TP2, are attached to the tergopleural tendon (O'Sullivan et al., 2018). Panels b and c show the inner structures and the illustrations of the wing hinge of *Rsl^{KO}* flies (with and without the downturned wing phenotype, respectively). Panel d shows those of the *Rsl^{KO}* fly with *Rsl*-GR. In Fig. 3E, the adults 72 h after eclosion were used for taking the photos, except for panel b for which adults 0 h after eclosion were used. Black arrowheads indicate the internal cuticle structure corresponding to the root of the wing hinge. White arrowheads indicate the tergopleural tendon devoid of any blue fluorescence signal in *Rsl^{KO}* flies. Asterisks indicate Dpy-YFP signals attached to flight muscles other than

TP-1 and TP-2. Scale bar: 50 µm.

Figure 4. Analyses of *Duox* functions in Rsl polymerization. (A) The wing postures of the control (*Rsl>GFP-IR*) and *Duox* knockdown flies (*Rsl>NIG 3131R-3*, and *Rsl>Duox-RNAi*$_{976–1145}$) are compared. Scale bar: 0.5 mm. (B) The temporal changes in the proportions of flies with normal wing posture after eclosion are shown. The flies used were the same as those in (A) (closed circles: *Rsl>GFP-RNAi*, grey closed circles: *Rsl>NIG3131R-3*, and gray open circles: *Rsl>Duox-RNAi*$_{976–1145}$). (C) Western blot analyses of Rsl protein levels were performed using samples from day-4-APF pupae to day-2-after-eclosion adults. The left and right are flies of the control (*Rsl>GFP-RNAi*) and *Duox* knockdown (*Rsl>NIG3131R-3*), respectively. (D) The inner structures of the wing hinge in the two control flies, *Rsl-Gal4/+* (panel a) and *NIG3131R-3/+* (panel b), are shown. The changes in the structure in the *Duox*-knockdown flies (*Rsl>NIG3131R-3*) are shown (panels c–e). Panel f on the right is the schematic of panel e. TP-1 and TP-2 muscles were stained with phalloidin. In *Duox*-knockdown flies, the dotted line (panel c) indicates the outline of the dityrosine signal corresponding to

the weak blue fluorescence signal indicated by triangles in the photo taken with a longer exposure time (panel d). Scale bar: 50 µm. (E) Wing posture of the *Duox* knockdown fly (*Rsl>NIG3131R-3*) and that of the *Duox* knockdown fly with the additional *TcDuox* expression (*Rsl> NIG3131R-3, TcDuox*). Scale bar: 0.5 mm. (F) Difference in the proportion changes of flies with normal wing posture was compared between *Rsl> NIG3131R-3, eGFP* (gray circle) and *Rsl>NIG3131R-3, TcDuox* (closed circle) flies. (G) Western blot analyses were performed to examine the levels of the Rsl protein from day-4-APF pupae to day-2-after-eclosion adults are shown. The left shows the *Duox*-knockdown individuals (*Rsl>NIG3131R-3, eGFP*) and the right shows the rescued individuals (*Rsl>NIG3131R-3, TcDuox*). (H) The photos and illustrations of the inner structure of the wing hinge in *Duox*-knockdown (left panels) and rescued flies (right panels) are shown. Scale bar: 50 µm (I) Western blot analyses of reRsl protein and dityrosine levels. reRsl was incubated in the presence (+) or absence (-) of 20 µg/µL horseradish peroxidase (HRP) and/or 0.3% hydrogen peroxide (H_2O_2) in 50 mM sodium phosphate buffer (pH 7.0) for 1 h at 30°C. Closed triangles show the signals stacking at the entry site of the concentration gels. Open triangle shows the signal stacking at the

border between the concentration and separation gels. Curly bracket shows smear signals in stacking gel.

Figure 5. Contributions of *Rsl* and *Duox* to fly's jumping. (A) Experimental scheme to measure jump distance of de-winged flies. (B) The jump distances between the control flies (*Rsl>GFP-RNAi*, white box) and *Rsl* knockdown flies (*Rsl>Rsl-RNAi*, gray box) are compared. Cross marks indicate the average. (Wilcoxon rank sum test, **: $P < 0.01$, *Rsl>GFP-RNAi*: n=8, *Rsl>Rsl-RNAi*: n=12). (C) The Rsl^{KO} phenotype of jump distance was rescued with *Rsl-GR*. The flies used were the wild-type (w^{1118}, white box), Rsl^{KO} (w^{1118}; Rsl^{KO}, gray box), and Rsl^{KO} with *Rsl-GR* (w^{1118}; Rsl^{KO}; *Rsl-GR*, dark gray box). Cross marks indicate the average (Wilcoxon rank sum test, Bonferroni correction, w^{1118}: n=10, Rsl^{KO}: n=10, Rsl^{KO} with *Rsl-GR*: n=11). (D) Effect of *Duox* knockdown on jump performance was examined. The graph shows the jump distances of the control flies (*Rsl>GFP-RNAi,* white box), the *Duox* knockdown flies (*Rsl> NIG 3131R-3*, indicated by the light gray box, and *Rsl>Duox-RNAi*$_{976–1145}$ indicated by the gray box) (Wilcoxon rank sum test, Bonferroni correction, *Rsl>GFP-RNAi*: n=9, *Rsl> NIG 3131R-3*: n=12,

Rsl>Duox-RNAi$_{976–1145}$: n=8). (E) The phenotype of *Duox* knockdown flies was rescued by the additional expression of *TcDuox*. The graph shows the jump distances of the *Duox* knockdown flies (*Rsl> NIG3131R-3, eGFP,* white box) and the flies with *TcDuox* expression (*Rsl> NIG3131R-3, TcDuox*, gray box) (Wilcoxon rank sum test, **: $P <$ 0.01, *Rsl> NIG3131R-3, eGFP*: n=9, *Rsl> NIG3131R-3, TcDuox*: n=7).

Figure 1

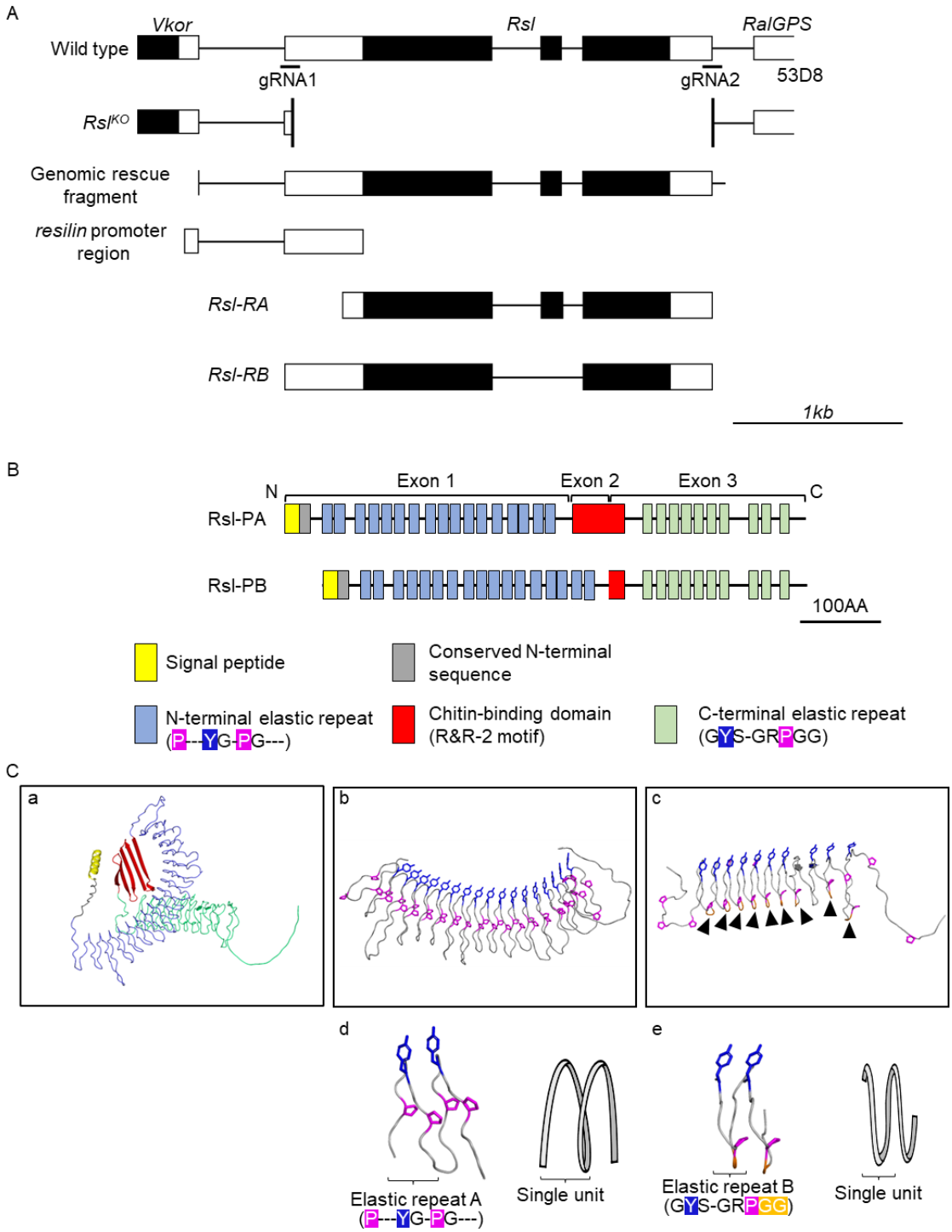
A
Vkor
Rsl
RalGPS
Wild type
gRNA1
gRNA2
53D8
RslKO
Genomic rescue fragment
resilin promoter region
Rsl-RA
Rsl-RB
1kb
B
N
Exon 1
Exon 2
Exon 3
C
Rsl-PA
Rsl-PB
100AA
Signal peptide
Conserved N-terminal sequence
N-terminal elastic repeat (P---YG-PG---)
Chitin-binding domain (R&R-2 motif)
C-terminal elastic repeat (GYS-GRPGG)
C
a
b
c
d
e
Elastic repeat A (P---YG-PG---)
Single unit
Elastic repeat B (GYS-GRPGG)
Single unit

Figure 2

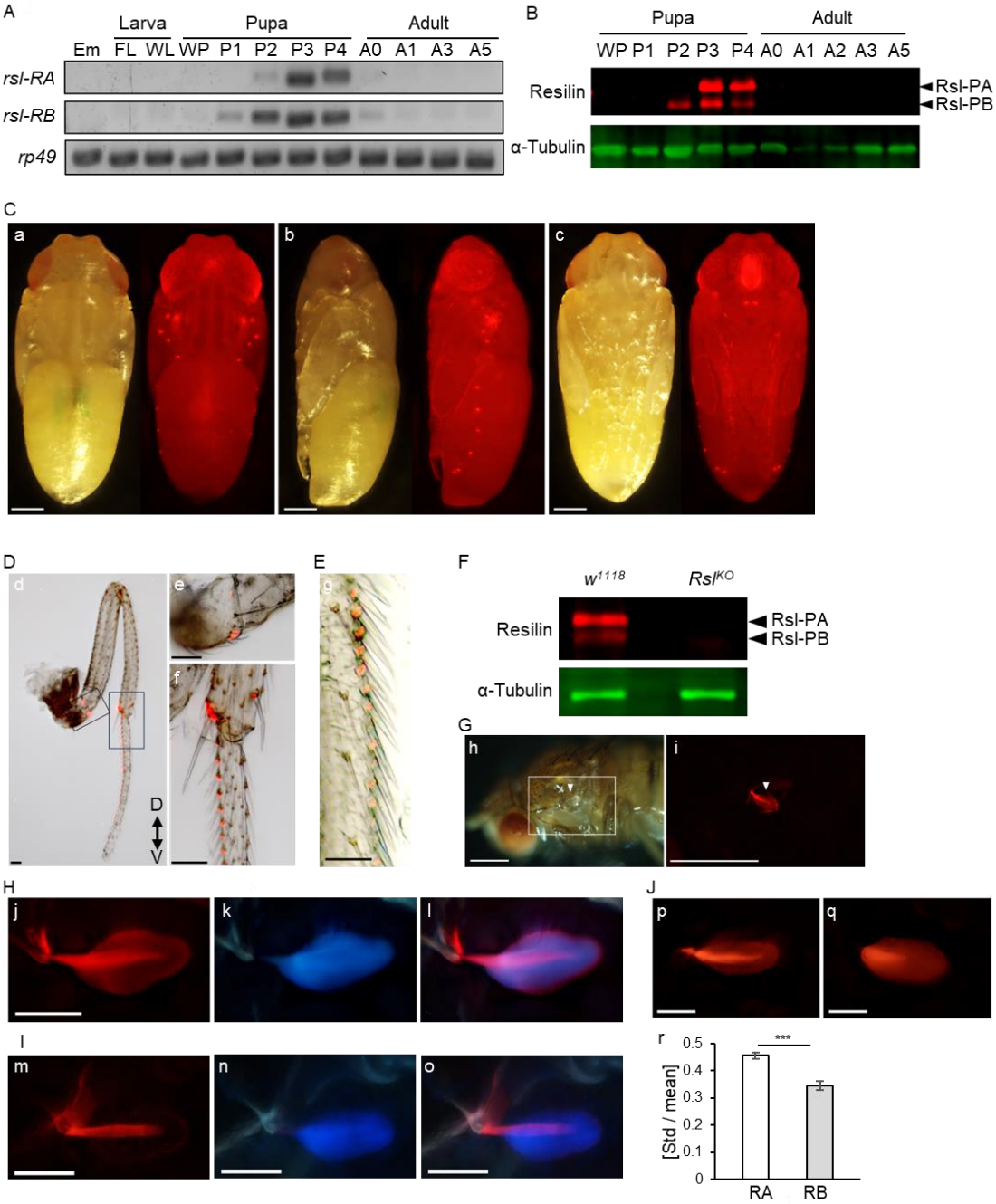
A
Larva
Pupa
Adult
Em FL WL WP P1 P2 P3 P4 A0 A1 A3 A5
rsl-RA
rsl-RB
rp49
B
Pupa
Adult
WP P1 P2 P3 P4 A0 A1 A2 A3 A5
Resilin
α-Tubulin
Rsl-PA
Rsl-PB
C
a
b
c
D
d
e
f
D
V
E
g
F
w1118
RslKO
Resilin
α-Tubulin
Rsl-PA
Rsl-PB
G
h
i
H
j
k
l
I
m
n
o
J
p
q
r
***
[Std / mean]
0.5
0.4
0.3
0.2
0.1
0
RA
RB

Figure 3

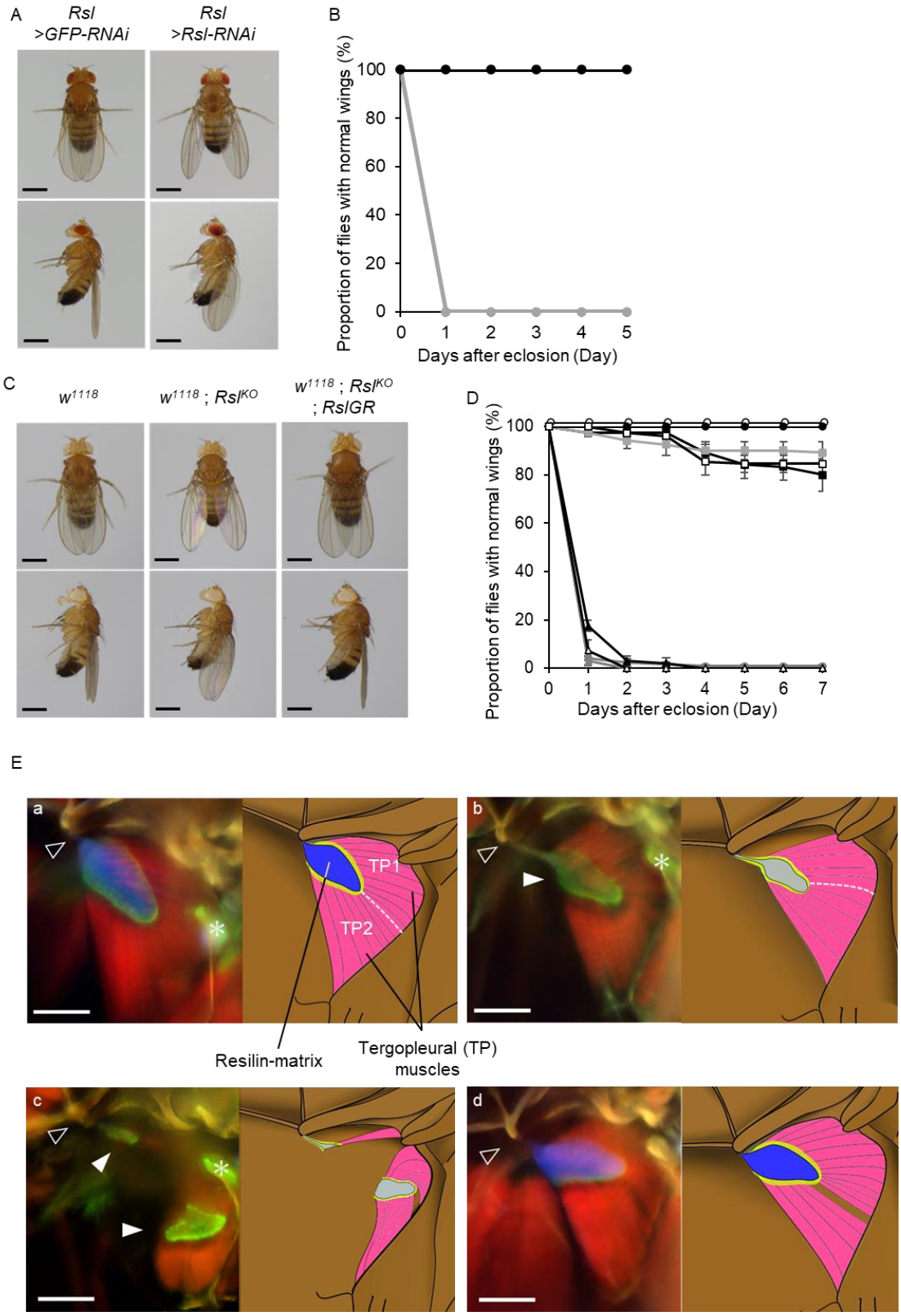
A
Rsl >GFP-RNAi
Rsl >Rsl-RNAi
B
Proportion of flies with normal wings (%)
100
80
60
40
20
0
0 1 2 3 4 5
Days after eclosion (Day)
C
w1118
w1118 ; RslKO
w1118 ; RslKO ; RslGR
D
Proportion of flies with normal wings (%)
100
80
60
40
20
0
0 1 2 3 4 5 6 7
Days after eclosion (Day)
E
a
TP1
TP2
Resilin-matrix
Tergopleural (TP) muscles
b
c
d

Figure 4-1

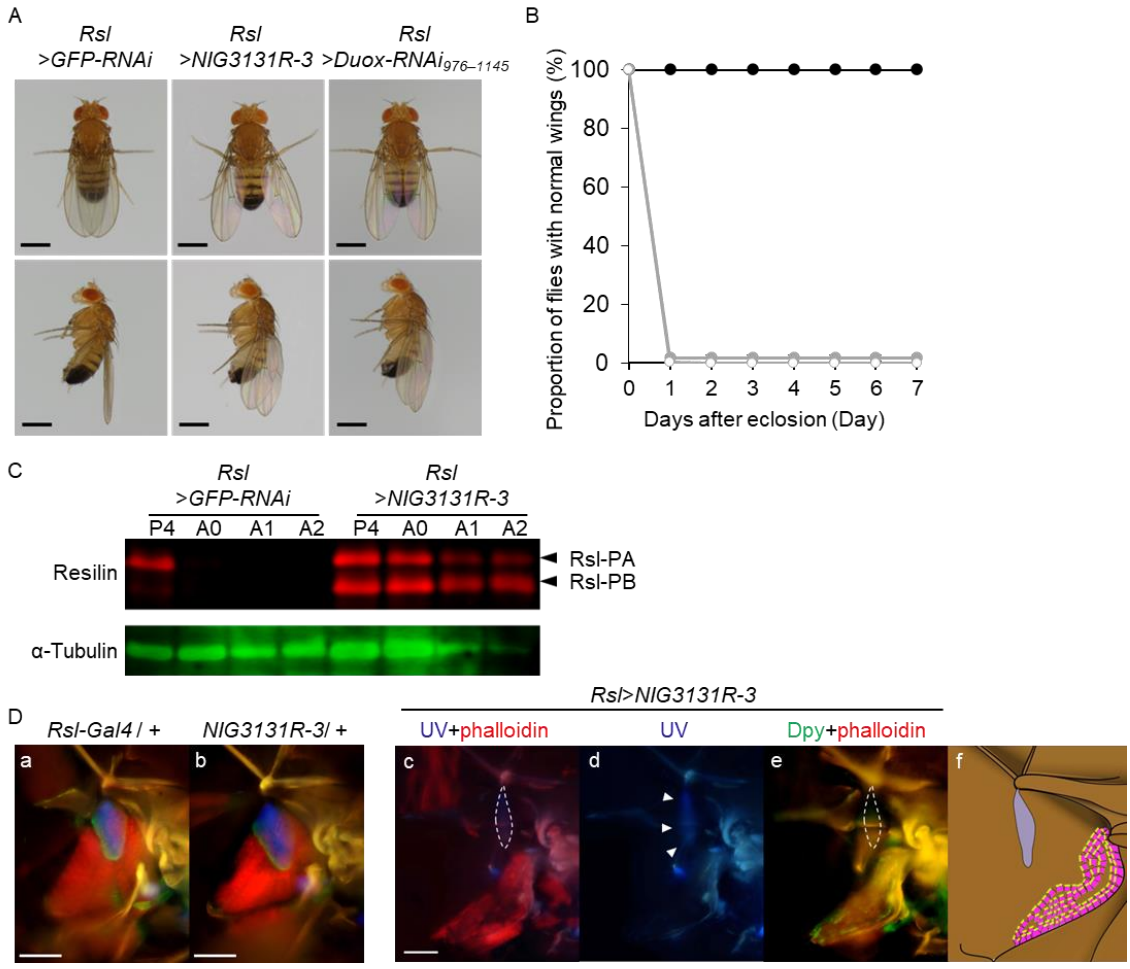
A
Rsl >GFP-RNAi
Rsl >NIG3131R-3
Rsl >Duox-RNAi976–1145
B
Proportion of flies with normal wings (%)
100
80
60
40
20
0
0 1 2 3 4 5 6 7
Days after eclosion (Day)
C
Rsl >GFP-RNAi
Rsl >NIG3131R-3
P4 A0 A1 A2 P4 A0 A1 A2
Resilin
Rsl-PA
Rsl-PB
α-Tubulin
D
Rsl-Gal4 / +
NIG3131R-3/ +
Rsl>NIG3131R-3
UV+phalloidin
UV
Dpy+phalloidin
a
b
c
d
e
f

Figure 4-2

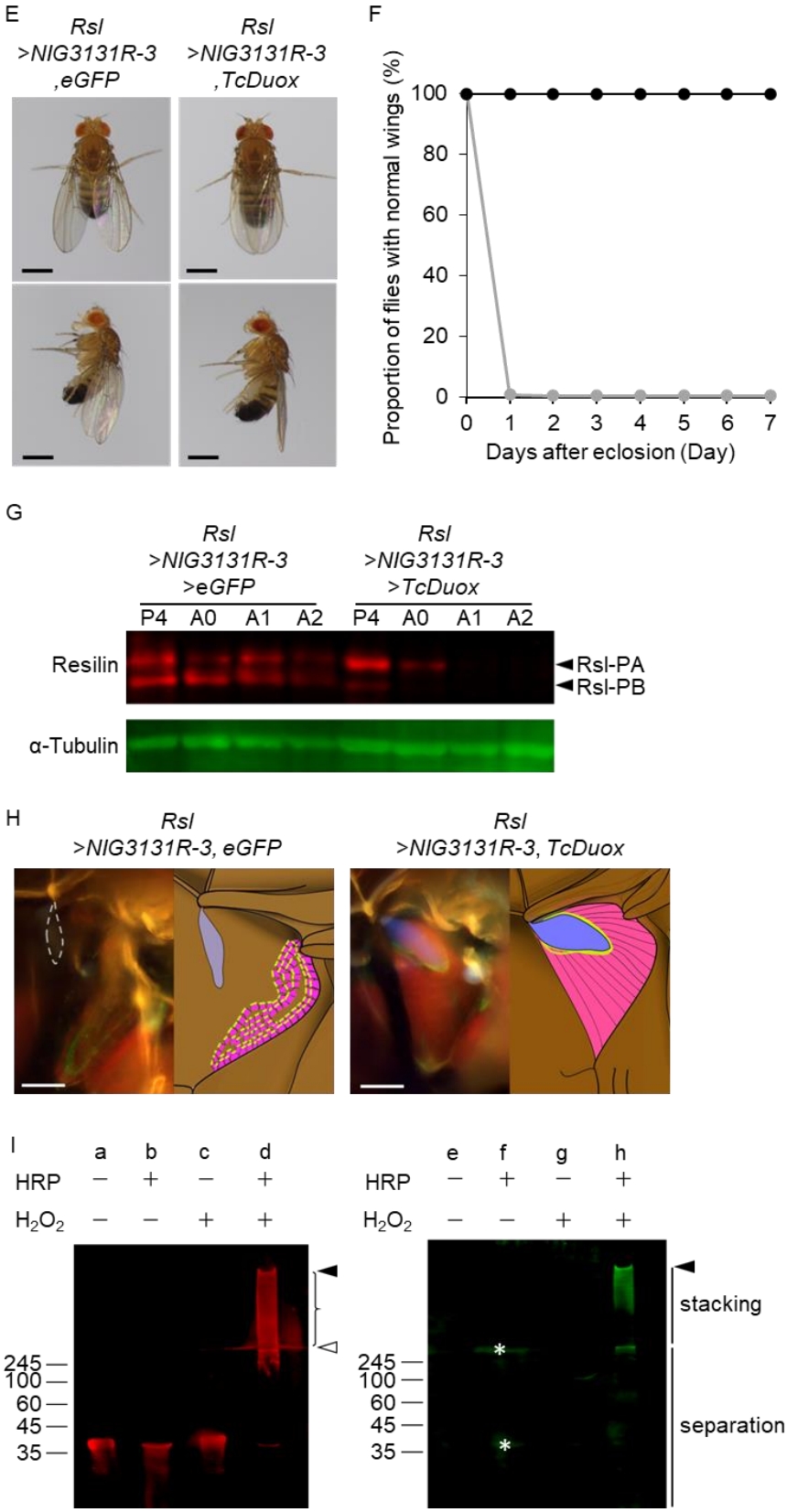
E
Rsl >NIG3131R-3 ,eGFP
Rsl >NIG3131R-3 ,TcDuox
F
Proportion of flies with normal wings (%)
100
80
60
40
20
0
0 1 2 3 4 5 6 7
Days after eclosion (Day)
G
Rsl >NIG3131R-3 >eGFP
Rsl >NIG3131R-3 >TcDuox
P4 A0 A1 A2 P4 A0 A1 A2
Resilin
Rsl-PA
Rsl-PB
α-Tubulin
H
Rsl >NIG3131R-3, eGFP
Rsl >NIG3131R-3, TcDuox
I
a b c d
HRP − + − +
H2O2 − − + +
245
100
60
45
35
e f g h
HRP − + − +
H2O2 − − + +
stacking
separation

Figure 5

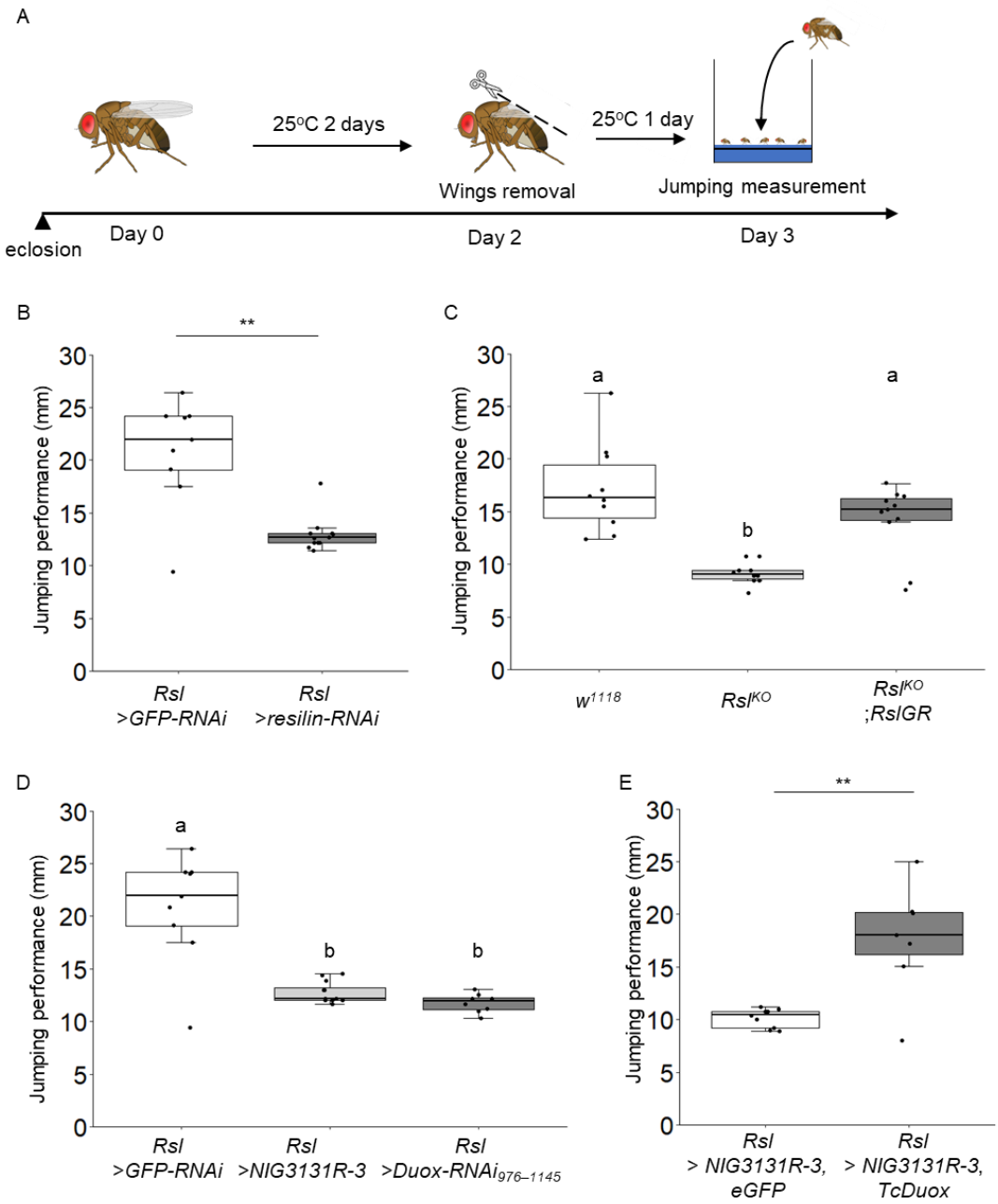
A
25°C 2 days
Wings removal
25°C 1 day
Jumping measurement
eclosion
Day 0
Day 2
Day 3
B
**
Jumping performance (mm)
Rsl >GFP-RNAi
Rsl >resilin-RNAi
C
a
b
a
Jumping performance (mm)
w1118
RslKO
RslKO ;RslGR
D
a
b
b
Jumping performance (mm)
Rsl >GFP-RNAi
Rsl >NIG3131R-3
Rsl >Duox-RNAi976–1145
E
**
Jumping performance (mm)
Rsl > NIG3131R-3, eGFP
Rsl > NIG3131R-3, TcDuox